Hindawi Publishing Corporation
Advances in Materials Science and Engineering
Volume 2013, Article ID 950791, 6 pages
http://dx.doi.org/10.1155/2013/950791

Research Article

Crack Detection in Single-Crystalline Silicon Wafer Using Laser Generated Lamb Wave

Min-Kyoo Song[1] and Kyung-Young Jhang[2]

[1] *Graduate School of Mechanical Engineering, Hanyang University, Seoul 133-791, Republic of Korea*
[2] *School of Mechanical Engineering, Hanyang University, Seoul 133-791, Republic of Korea*

Correspondence should be addressed to Kyung-Young Jhang; kyjhang@hanyang.ac.kr

Received 19 July 2013; Revised 16 November 2013; Accepted 18 November 2013

Academic Editor: Yan Yang

Copyright © 2013 M.-K. Song and K.-Y. Jhang. This is an open access article distributed under the Creative Commons Attribution License, which permits unrestricted use, distribution, and reproduction in any medium, provided the original work is properly cited.

In the semiconductor industry, with increasing requirements for high performance, high capacity, high reliability, and compact components, the crack has been one of the most critical issues in accordance with the growing requirement of the wafer-thinning in recent years. Previous researchers presented the crack detection on the silicon wafers with the air-coupled ultrasonic method successfully. However, the high impedance mismatching will be the problem in the industrial field. In this paper, in order to detect the crack, we propose a laser generated Lamb wave method which is not only noncontact, but also reliable for the measurement. The laser-ultrasonic generator and the laser-interferometer are used as a transmitter and a receiver, respectively. We firstly verified the identification of S0 and A0 lamb wave modes and then conducted the crack detection under the thermoelastic regime. The experimental results showed that S0 and A0 modes of lamb wave were clearly generated and detected, and in the case of the crack detection, the estimated crack size by 6 dB drop method was almost equal to the actual crack size. So, the proposed method is expected to make it possible to detect the crack in the silicon wafer in the industrial fields.

1. Introduction

Semiconductors have been applied to many fields including smart TVs, smart phones, smart PCs, automobiles, home appliances, and laptop computers. These fields have demanded that the semiconductor should be of high performance, high capacity, high reliability, small components, and low cost. Because of these demands, semiconductor fabrication processes have focused on the lithography for a nanometer-scaled line width. And especially, semiconductor packaging processes have focused on a few trends in recent years: multistacking components and thinner wafers [1–3]. The multistacking component implies that more chips have to be stacked up within the same size component for the high capacity, and the thinner wafer indicates that wafer thickness has to be very thin up to 30 μm for the multistacking component. Moreover, an attempt to change from 12 inch-wafers to 18 inch-wafers is recently going on, since larger wafers which are able to put more chips have impact on the yield improvement. Because of these trends that wafers are getting thinner and larger, silicon wafers are vulnerable to cracks during manufacturing. The cracks can also lead to the yield drop and reliability failure. Therefore, one of the most critical issues in the semiconductor packaging process is the crack. So, the online crack detection in silicon wafers is becoming more important than ever before and its importance cannot be stressed enough.

Previous articles about the online crack detection which deals with poly-crystalline silicon wafers commonly used in the solar cell industry are largely classified into two groups. One is the contact method by resonance ultrasonic vibrations and impact tests [4, 5]. The other is the noncontact method by an air-coupled ultrasonic lamb wave [6]. Resonance ultrasonic vibrations method can accurately detect the millimeter-length cracks and the impact testing method can also analyze defective wafers. But both of them are driven by external forces which are not adequate for thin silicon wafers under 100 μm thickness used generally. Air-coupled ultrasonic lamb wave method demonstrates the crack detection successfully and lamb wave is suitable for the thin silicon wafer. However,

this method has the problem of high impedance mismatches which cause dissipation of most incident energies from the surface of materials. This is also not satisfied for very noisy environment caused from facilities or manufacturing machines.

For many years, laser-ultrasonic technology has been increasingly used for nondestructive crack detections [7–10]. The biggest advantage of this technology is noncontact without regard to external forces and surface conditions of materials. This technology has another advantage that can reduce the energy loss by adjusting the shape of the laser beam for the energy enhancement. Although laser-ultrasonic technology has these advantages, few studies have performed for the crack detection in silicon wafers. Therefore, we propose the laser generated lamb wave method, which not only is noncontact but also guarantees the reliable measurement. And this paper deals with single crystalline silicon wafers commonly used in the semiconductor industry other than previous papers which deal with poly-crystalline silicon wafers.

Laser-ultrasonic technology has two main regimes. One is thermoelastic regime and the other is ablation regime [11]. In the case of thermoelastic regime, the ultrasonic waves are generated from thermoelastic expansions of materials. Meanwhile, in the case of ablation regime, the ultrasonic waves are generated from the material removal. If the ablation regime is applied to silicon wafers, they will be damaged. So, thermoelastic regime has to be applied to silicon wafers in terms of the reliability. And also there are two possible generation mechanisms; thermal effect and electrostriction. However, the thermal effect is dominant at the high power input while the electrostriction is dominant at the low power input [12]. In our case, the input power was in the range of high power input, so that we did not consider the electrostriction effect.

If the thermoelastic regime is applied to a silicon wafer that has the comparable thickness to wavelength, lamb wave is generated. We are expected to detect the cracks in silicon wafers through analysis of this lamb wave.

2. Dispersion Curves of Lamb Wave in Silicon Wafer

Lamb wave is dispersive, which implies that the wave velocity is dependent on the frequency. So dispersion curves need to be analyzed first. The wave velocities in single-crystalline silicon wafers are listed in Table 1. The silicon wafer has three kinds of different velocities depending on the orientations [13]. But, since wafers have the characteristics that cracks are easily initiated and cleft in the (110) orientation, it is reasonable to consider only the (110) orientation in terms of easier experiments. Figure 1 shows dispersion curves of group velocity which are plotted from velocities at the (110) orientation in the silicon wafer whose thickness is 525 μm. The curves in the dotted box area are mostly used for the practical applications, because other areas are more complicated. So the curves in this box area are supposed to be used for our experiments as well.

Table 1: Wave velocities in single-crystalline silicon wafer.

Orientation	Longitudinal wave velocity	Shear wave velocity
(100)	8436 (m/s)	5847 (m/s)
(110)	9138 (m/s)	4675 (m/s)
(111)	9360 (m/s)	5096 (m/s)

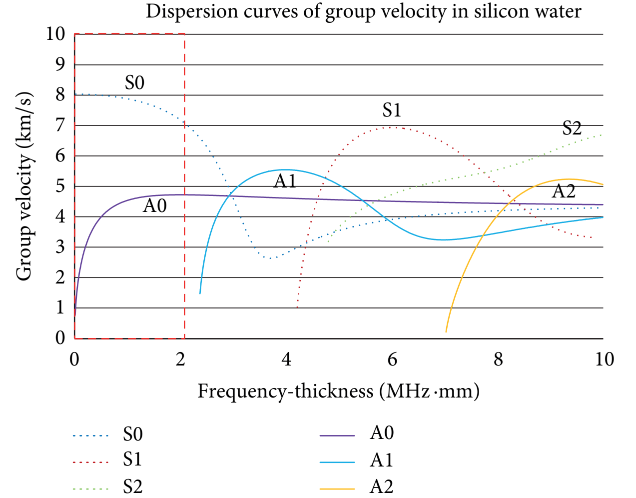

Figure 1: Dispersion curves of group velocity in silicon wafers whose thickness is 525 μm.

3. Simulation

The thermoelastic mechanism is described by a few equations. First, the laser energy that has Gaussian spatial and temporal distributions is quickly absorbed in the wafer as shown in Figure 2. This process can be expressed as

$$Q = 2\frac{E(1-R)}{S\tau}\exp\left(-2\frac{x^2}{r^2}\right)\exp\left(2.7726\frac{(t-2\tau^2)}{\tau^2}\right), \quad (1)$$

where Q means the heat source; E is the initial laser energy; R is the reflectivity; S is the surface area on which the laser is absorbed; τ is the pulse duration; r indicates a distance that laser density is $1/2$ times from the center; x is the spatial coordinates; t means time.

And then, the absorbed energy makes the temperature of the wafer increase sharply. The thermal conduction is caused by this large temperature gradient. This thermal conduction equation can be described as

$$\rho C_p \frac{\partial T}{\partial t} + \rho C_p u \nabla T = \nabla (k \nabla T) + Q, \quad (2)$$

where ρ, C_p, and T are density, heat capacity, and temperature, respectively; u means the displacement; Q is the heat generated from the heat source.

Table 2: Properties of the wafer.

Properties	Value						Unit
Reflectivity	0.32						
Density	2330						kg/m^3
Coefficient of thermal expansion	2.6×10^{-6}						1/K
Thermal conductivity	130						W/(m·K)
Heat capacity at constant pressure	700						J/(kg·K)
Elasticity matrix	166	64	64	0	0	0	GPa
	64	166	64	0	0	0	
	64	64	166	0	0	0	
	0	0	0	80	0	0	
	0	0	0	0	80	0	
	0	0	0	0	0	80	

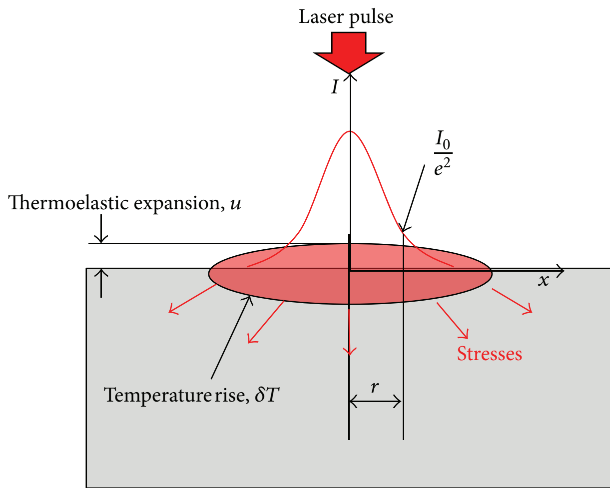

Figure 2: Schematic of thermoelastic mechanism.

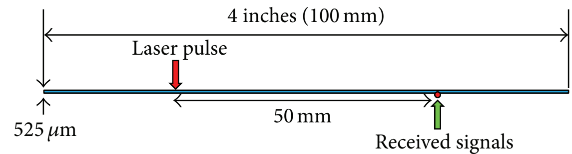

Figure 3: Geometrical dimensions of simulation model.

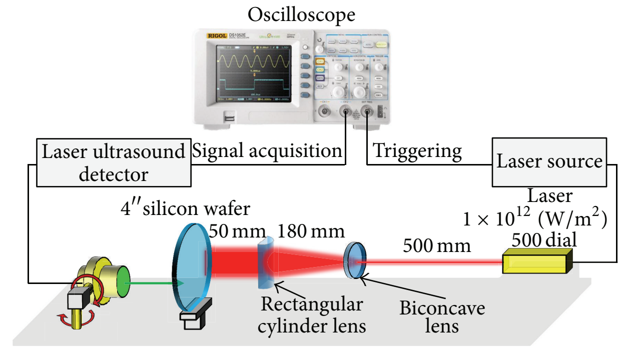

Figure 4: Experimental setup.

At last, thermoelastic expansion is caused by the large temperature gradient. Thermoelastic stresses are finally generated and thermoelastic wave is rapidly propagated. This equation of motion can be represented as

$$(\lambda + 2\mu)\nabla(\nabla \cdot u) - \mu\nabla \times \nabla \times u - \alpha(3\lambda + 2\mu)\nabla T = \rho\frac{\partial^2 u}{\partial t^2}, \quad (3)$$

where λ and μ are Lamé constants; α is coefficient of thermal expansion.

All of these equations were applied to the simulation with COMSOL multiphysics 4.3. The incident laser density and the pulse duration were adopted as 1.00×10^{12} W/m^2 and 5 ns. And we considered the line beam as the elliptical beam which has 11.5 mm major axis and 0.5 mm minor axis, as shown in the next experiment section. Other properties used in the simulation are listed in Table 2. The geometrical dimensions of this simulation were modeled as shown in Figure 3: the diameter of the wafer, 4 inches and the thickness of the wafer, 525 μm. The outside boundaries were considered as thermal insulations. And the mesh size was determined as 0.1 mm which is less than a 10th of the A0 mode wavelength and is small enough to get reasonable calculation accuracy [14]. Lamb wave was obtained at a distance of 50 mm from the laser source in this simulation.

4. Experimental Procedures and Setup

We conducted two experiments that are mode identification and crack detection. Firstly, lamb wave modes were identified in the wafer without any crack, as comparing the experiment and the simulation. Secondly, the modes which were identified in the first experiment were used for the crack detection experiment in the wafer with an artificial crack.

Figure 4 illustrates the experimental setup. The materials we used for two experiments are (100) single-crystalline silicon wafers that are manufactured by ShinEtsu Chemical

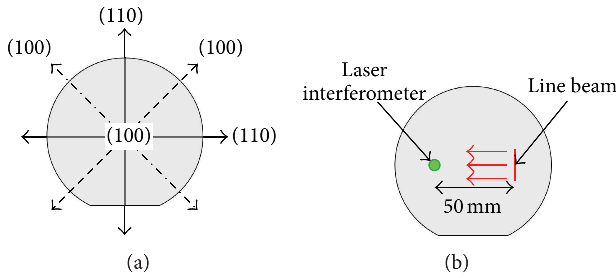

Figure 5: (a) Orientation in a (100) wafer and (b) the setup of the laser source and the laser interferometer.

Co., Ltd. The diameter and thickness of the wafers are 4 inches and 525 μm, respectively, which are the same in the previous simulation section. The pulsed laser made by Spectron Laser Systems was used as a transmitter. Its fundamental wavelength, beam diameter, pulse duration, and the repetition rate are 1064 nm, 4 mm, 5 ns, and 1 Hz, respectively. The laser interferometer made by TECNAR was used as a receiver. Its operating principle is described by two-wave mixing. This equipment detects out-of-plane displacement and the frequency bandwidth for the detection of lamb wave has upper limit, 2 MHz. An oscilloscope was used for triggering and signal acquisition.

Two lenses, which are able to transform the laser beam into a line beam, were used to make it clear to generate lamb wave: a biconcave lens and a rectangular cylinder lens. The biconcave lens was placed at a distance of 500 mm from the laser and then the distance between the biconcave lens and the rectangular cylinder lens was set to 180 mm, in order to make a beam diameter of 23 mm. The silicon wafer was located where the laser beam became a line beam whose width was 1 mm and length was 23 mm. Its distance was 50 mm from the rectangular cylinder lens. The laser intensity of the line beam was 1.00×10^{12} W/m^2, which is within the thermoelastic regime and less than the ablation threshold. The laser interferometer was installed behind the wafer due to the interference with other equipment. The oscilloscope was linked both to the laser source for the triggering and to the laser interferometer for the signal acquisition.

5. Mode Identification

The experimental setup for the mode identification was the same as in Figure 4. In addition, the orientation of the wafer was taken into account, because we supposed to only consider the (110) orientation where cracks are easily generated. Figure 5(a) illustrates the orientations in a (100) wafer. The line beam as a laser source was aligned perpendicular to the flat zone of the wafer, in order to generate lamb wave in the direction, (110), as shown in Figure 5(b) which describes the setup of the laser source and the laser interferometer.

In the case of the experimental result, the triggering signal is occupied by around 4 μs as shown in Figure 6(a). We can also see that S0 mode and A0 mode are clearly generated and received. S0 mode is received in 6.24 μs and A0 mode is measured from 8.5 μs to 18 μs.

In the case of the simulation result, S0 mode and A0 mode are also obviously generated and received. S0 mode is obtained in 6.6 μs and A0 mode is followed for the time which is similar to the experimental result, as shown in Figure 6(b).

As comparing the experiment with the simulation, the arrival times of S0 mode are almost the same. Likewise, the arrival times of A0 mode are also the same. In terms of the velocity, S0 mode is faster than A0 mode. In terms of the amplitude, however, it can be seen from both results that the amplitude of A0 mode is much larger than that of S0 mode. This is because A0 mode is dominant for out-of-plane on the surface of the wafer; on the other hand, S0 mode is dominant for in-plane on the surface of the wafer. Note that the equipment used for the receiver detects only the out-of-plane displacement. As a result of plotting the STFT result overlapped with the group velocity, A0 mode strongly appears around 500 kHz as shown in Figure 7. It implies that A0 mode is helpful for the crack detection.

However, considering that the nondispersive wave is preferable for the easier interpretation of wave signal, the higher frequency band of 2~4 MHz looks better as we can see from the dispersion curve of A0 mode shown in Figure 7. But, in our experimental setup, the upper frequency limit of lamb wave detector was 2 MHz and the line beam width 1 mm was the least width for the safe generation in the thermoelastic regime. Thus, we did not have much flexibility to choose the frequency band.

In order to use the higher frequency lamb wave for the inspection, both sides of generation and detection should be considered. In the generation side, a simple way is the reduction of the line beam width. But, in this case, there exists a limit in the input laser power to keep the laser intensity of line beam within the thermoelastic range. In the detection side, the frequency bandwidth and the sensitivity should be considered. The frequency bandwidth of lamb wave detector is dependent on the beam spot size of detection laser. The smaller spot size can detect the higher frequency (or the shorter wavelength) lamb wave. Also, if we reduce the generation laser power to make the line beam width smaller within the thermoelastic regime, then the generated wave amplitude will be decreased. In this case, the higher sensitivity of detector may be required.

6. Crack Detection

A0 mode was used for the crack detection because of the large amplitude, as was mentioned in the former section. The experimental setup was nothing different from the setup for the mode identification. But, it is the difference that the reflection method was used by scanning the wafer that has the crack artificially made with a diamond cutter, as shown in Figure 8. The crack length, width, and depth are 5 mm, 0.5 mm, and 0.1 mm, respectively.

We analyzed what kinds of modes are generated in the center of the crack prior to the crack detection experiment. The crack, the laser interferometer, and the line beam were positioned as shown in Figure 9(a). And then a variety of modes were received as shown in Figure 9(b). S0 mode arrives the earliest at 2.5 μs, but this is buried in the triggering

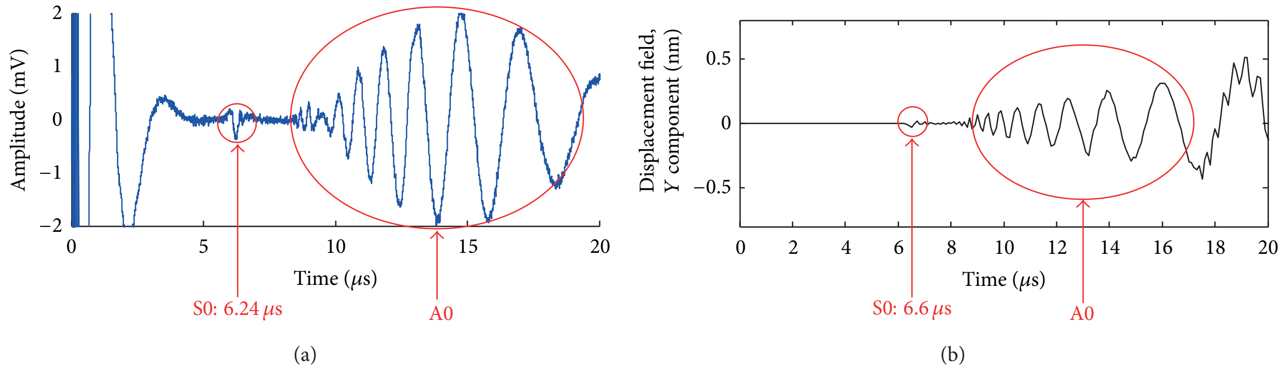

Figure 6: (a) Experimental result and (b) simulation result for mode identification.

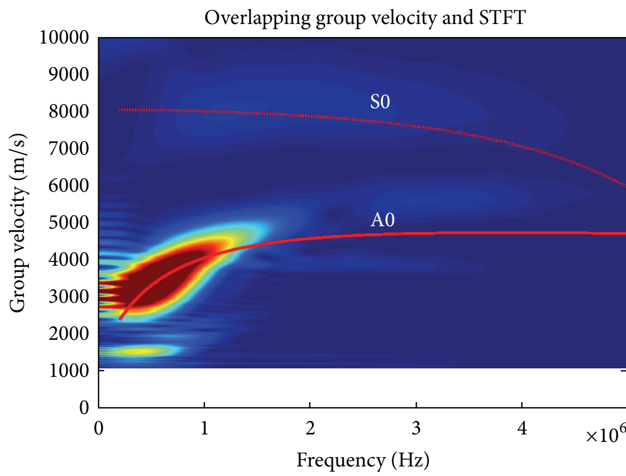

Figure 7: STFT result overlapped with group velocity.

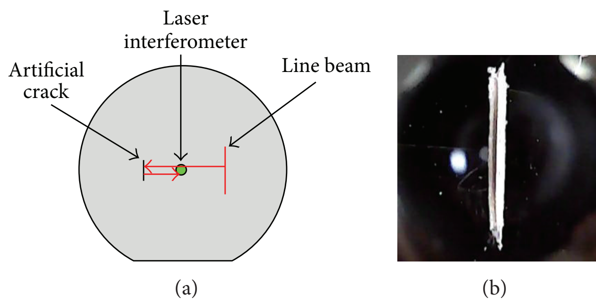

Figure 8: (a) Reflection method schematic and (b) artificial crack.

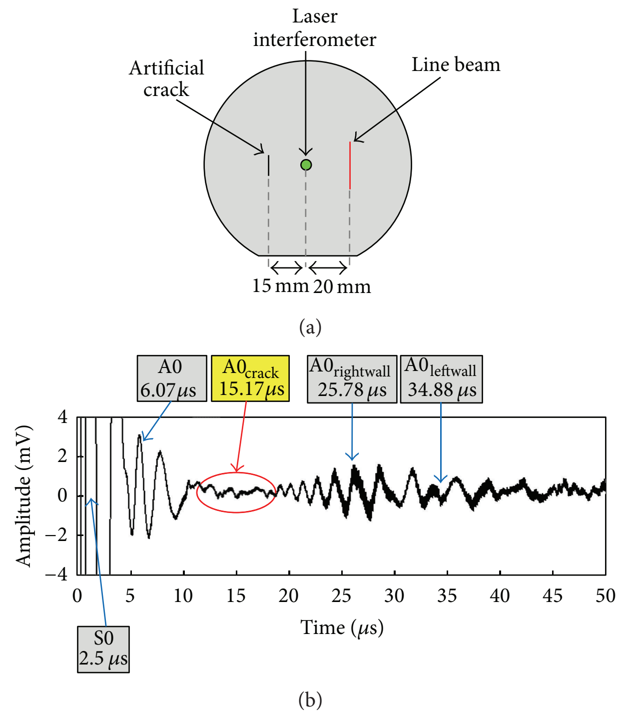

Figure 9: (a) Experimental setup and (b) received signals.

signal. Since S0 mode has very tiny amplitude, it will not be considered any more. And A0 mode arrives then at 6.07 μs. Some part of A0 mode is also buried in the triggering signal. Next, A0 mode reflected from the crack is detected at 15.17 μs. This is what we are looking for in this experiment. And then, the complicated signals are followed. So the reflected A0 mode from the crack is analyzed for the crack detection and its signal is in the range from 12 to 18 μs.

The crack was scanned with every 0.5 mm and the scan length was 10 mm as shown in Figure 10(a). So every datum corresponding to each A0 mode reflected from the crack was extracted and plotted based on the maximum amplitude in the range from 12 to 18 μs. And then the 6 dB drop method is applied to decide the defect size, which has been widely used for the defect sizing based on the ultrasonic scan [15, 16]. Figure 10(b) shows the experimental result that the estimated crack length by 6 dB drop method is about 4.8 mm. In comparison with the actual crack length, 5 mm, we come to conclusion that the width more than 50% of the maximum signal level can be considered as an actual crack length. Therefore, the proposed method is expected to make it possible for the online crack detection in the silicon wafer.

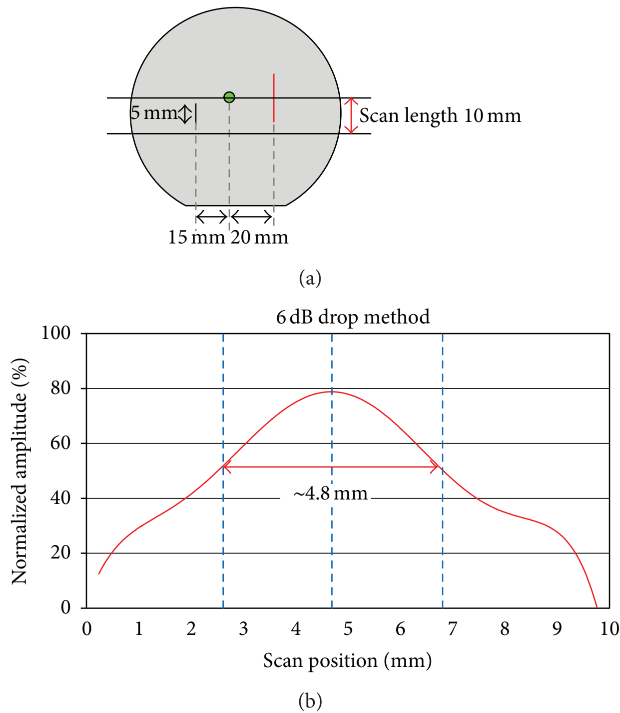

FIGURE 10: (a) Scan length and (b) experimental result by 6 dB drop method.

7. Conclusions

This paper proposed the laser generated Lamb wave which not only is noncontact method, but also guarantees the reliable measurement, in order to detect the crack in the single-crystalline silicon wafer. We verified the identification of S0 and A0 lamb wave modes and then conducted crack detection under the thermoelastic regime. At first, mode identification was carried out, as comparing the experiment with the simulation. The experimental result showed a good agreement with the simulation result. In particular, we could see that the amplitude of A0 mode is remarkably larger than that of S0 mode. This is because A0 mode is dominant for out-of-plane; on the other hand, S0 mode is dominant for in-plane. So A0 mode was used for the crack detection. It can be seen that the actual crack size was nearly identical to the estimated crack size by 6 dB drop method, as the crack was scanned. Finally, we concluded that laser generated lamb wave we proposed can be used for the crack detection in silicon wafer.

Although this paper deals with a single-crystalline silicon wafer as the beginning of the crack detection, our future work will deal with an individual chip separated from a thinner wafer by a saw machine.

Acknowledgment

This work was financially supported by the National Research Foundation of Korea (NRF) as a grant funded by the Korean government (NRF-2013M2A2A9043241).

References

[1] E.-K. Kim, "Assessment of ultra-thin Si wafer thickness in 3D wafer stacking," *Microelectronics Reliability*, vol. 50, no. 2, pp. 195–198, 2010.

[2] C.-C. A. Chen and L.-S. Hsu, "A process model of wafer thinning by diamond grinding," *Journal of Materials Processing Technology*, vol. 201, no. 1-3, pp. 606–611, 2008.

[3] Y. S. Kim, N. Maeda, H. Kitada et al., "Advanced wafer thinning technology and feasibility test for 3D integration," *Microelectronic Engineering*, vol. 107, pp. 65–71, 2013.

[4] W. Dallas, O. Polupan, and S. Ostapenko, "Resonance ultrasonic vibrations for crack detection in photovoltaic silicon wafers," *Measurement Science and Technology*, vol. 18, no. 3, article 038, pp. 852–858, 2007.

[5] C. Hilmersson, D. P. Hess, W. Dallas, and S. Ostapenko, "Crack detection in single-crystalline silicon wafers using impact testing," *Applied Acoustics*, vol. 69, no. 8, pp. 755–760, 2008.

[6] S. K. Chakrapani, M. J. Padiyar, and K. Balasubramaniam, "Crack detection in full size Cz-silicon wafers using lamb wave air coupled ultrasonic testing (LAC-UT)," *Journal of Nondestructive Evaluation*, vol. 31, pp. 46–55, 2012.

[7] C. Ni, Y. Shi, Z. Shen, J. Lu, and X. Ni, "An analysis of angled surface-breaking crack detection by dual-laser source generated ultrasound," *NDT and E International*, vol. 43, no. 6, pp. 470–475, 2010.

[8] S. Dixon, S. E. Burrows, B. Dutton, and Y. Fan, "Detection of cracks in metal sheets using pulsed laser generated ultrasound and EMAT detection," *Ultrasonics*, vol. 51, no. 1, pp. 7–16, 2011.

[9] C. Ni, L. Dong, Z. Shen, and J. Lu, "The experimental study of fatigue crack detection using scanning laser point source technique," *Optics and Laser Technology*, vol. 43, no. 8, pp. 1391–1397, 2011.

[10] S. J. Davies, C. Edwards, G. S. Taylor, and S. B. Palmer, "Laser-generated ultrasound: its properties, mechanisms and multifarious applications," *Journal of Physics D*, vol. 26, no. 3, pp. 329–348, 1993.

[11] C. B. Scruby and L. E. Drain, *Laser Ultrasonics: Techniques and Applications*, Adam Hilger, Bristol, UK, 1990.

[12] H. J. Shin, S. W. Noh, J. H. Lee, and J. S. Jang, "Pulsed laser induced photoacoustic effect in silicon, mainly caused by thermal expansion and electrostriction, is studied," *Journal of the Institute of Electronics Engineers of Korea*, vol. 3, pp. 42–44, 1988.

[13] J. J. Wortman and R. A. Evans, "Young's modulus, shear modulus, and poisson's ratio in silicon and germanium," *Journal of Applied Physics*, vol. 36, no. 1, pp. 153–156, 1965.

[14] H.-X. Sun, S.-Y. Zhang, and B.-Q. Xu, "Influence of viscoelastic property on laser-generated surface acoustic waves in coating-substrate systems," *Journal of Applied Physics*, vol. 109, no. 7, Article ID 073107, 2011.

[15] J. Blitz and G. Simpson, *Ultrasonic Methods of Non-Destructive Testing*, Chapman and Hall, London, UK, 1996.

[16] P. Ciorau, "Comparison between -6 dB and -12 dB amplitude drop techniques for length sizing," Ontario Power Generation, no. 11, 2011, http://www.ndt.net/.

Journal of
Nanotechnology

International Journal of
Corrosion

International Journal of
Polymer Science
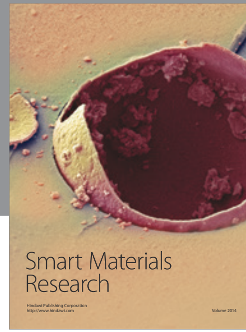
Smart Materials
Research
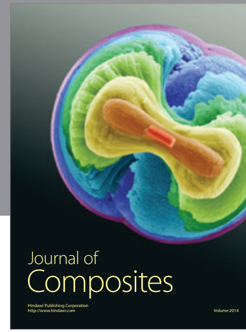
Journal of
Composites

BioMed
Research International

Hindawi
Submit your manuscripts at
http://www.hindawi.com
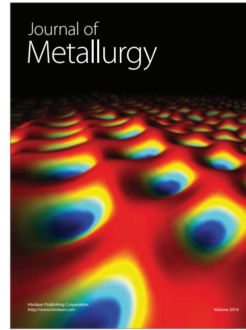
Journal of
Metallurgy

Journal of
Materials
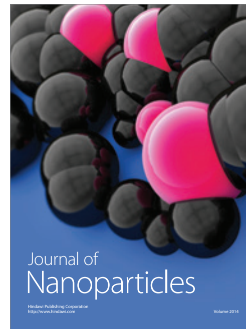
Journal of
Nanoparticles
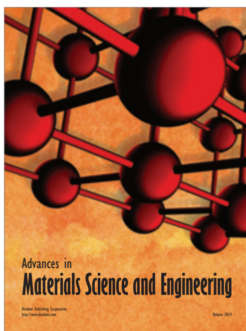
Advances in
Materials Science and Engineering
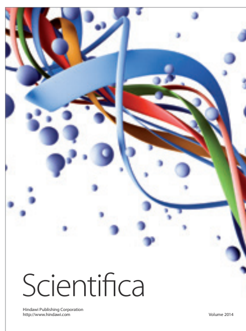
Scientifica
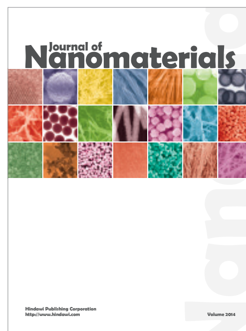
Journal of
Nanomaterials
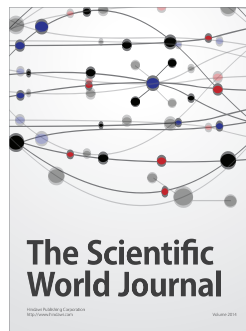
The Scientific
World Journal

International Journal of
Biomaterials

Journal of
Nanoscience

Journal of
Coatings

Journal of
Crystallography

Journal of
Ceramics
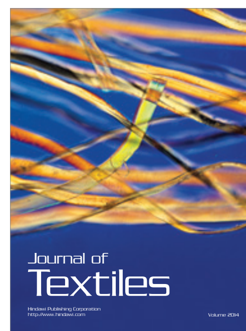
Journal of
Textiles